AIAA JOURNAL
Vol. 42, No. 3, March 2004

Flow Structure on a Delta Wing of Low Sweep Angle

B. Yaniktepe* and D. Rockwell†
Lehigh University, Bethlehem, Pennsylvania 18015

The instantaneous and averaged flow structure past a delta wing of low sweep angle is investigated using a technique of high-image-density particle image velocimetry. Emphasis is on crossflow planes, where vortex breakdown and stall occur, and the identification of buffeting mechanisms in these regions. At all values of angle of attack up to the fully stalled condition, the averaged vorticity layer exhibits an elongated form; the classical (single) large-scale concentration of vorticity within the leading-edge vortex of a highly swept wing is not present. At low angle of attack α, this elongated, averaged layer can exhibit, however, well-defined concentrations of vorticity. These elongated vorticity layers are accompanied by narrow recirculation zones adjacent to the wing surface. Furthermore, the averaged streamline topology exhibits, at lower α, a saddle point located slightly outboard of the leading edge, in contrast to a saddle point located on the plane of the symmetry of a highly swept wing. Patterns of velocity fluctuation and Reynolds stress show peaks that are generally coincident with large values of averaged vorticity, which indicates that they arise from unsteady events in regions of high shear. Well-defined concentrations of instantaneous vorticity can be identified at all values of angle of attack α. At low α individual concentrations retain their identity, but at moderate and high α larger-scale clusters of instantaneous vorticity occur. In turn, these patterns of vorticity are in accord with the time-averaged spectra of the fluctuating velocity; the predominant peaks of such spectra take on lower values in regions where larger-scale clusters of vorticity appear. Control in the form of a small amplitude perturbation of the wing, at a frequency corresponding to the subharmonic of the spectral component in the initial region of development of the separated layer, can restabilize the time-averaged patterns of streamline topology and vorticity, such that they resemble those occurring at lower angle of attack α.

Nomenclature

C	=	root chord, mm
f	=	frequency, Hz
f_0	=	frequency of spectral peak of velocity fluctuation, Hz
S	=	local semispan of wing, mm
T	=	period of perturbed angle of attack α, deg
U	=	freestream velocity, mm/s
V	=	magnitude of velocity vector, mm/s
v'	=	instantaneous velocity fluctuation in direction parallel to surface of wing, mm/s
w'	=	instantaneous velocity fluctuation normal to surface of wing, mm/s
w_{rms}	=	rms of velocity fluctuation, mm/s
x	=	distance from apex measured along plane of symmetry of wing, mm
x'_b	=	distance from apex measured along axis of leading-edge vortex, mm
y	=	distance from apex measured normal to plane of symmetry of wing, mm
α	=	angle of attack, deg
$\Delta\alpha$	=	perturbation of angle of attack α, deg
Λ	=	sweep angle, deg
λ	=	wavelength between vorticity concentrations, mm
ψ	=	streamfunction, mm^2
ω	=	vorticity, 1/s
$\langle\ \rangle$	=	time-averaged value of quantity

Received 28 March 2003; revision received 8 September 2003; accepted for publication 9 September 2003.

*Visiting Scientist, Department of Mechanical Engineering and Mechanics; currently Research Assistant, Department of Mechanical Engineering, Cukurova University, Adana, Turkey.

†Paul B. Reinhold Professor, Department of Mechanical Engineering and Mechanics, 356 Packard Laboratory, 19 Memorial Drive West. Member AIAA.

I. Introduction

In recent years, considerable insight has been gained into the averaged and unsteady structure on delta wings having relatively large sweep angle. These investigations, which are described in the following, serve as a basis for interpretation of the flow structure on wings of moderate sweep angle, which is the focus of the present investigation.

A. Large-Scale Patterns of Flow Structure

Global experimental techniques, such as particle image velocimetry (PIV), have provided a basis for interpretation of the averaged crossflow structure on highly swept wings. Regarding the streamline topology, Magness et al.[1] defined, via PIV, the critical points associated with the leading-edge vortices having spiral streamline patterns with well-defined centers. A saddle point, that is, an apparent intersection of streamlines, occurred at the plane of symmetry of the wing. At sufficiently high angle of attack, however, the streamline pattern exhibits features not characteristic of a classical leading-edge vortex. Visbal and Gordnier[2] performed related numerical simulations, which yielded interpretation of the various topologies of streamline patterns on highly swept delta wings.

Topological representations of the flow on the basis of streamlines are linked to patterns of vorticity on the crossflow plane. A well-known feature on wings of high sweep angle is the existence of a large-scale vorticity concentration at the apparent center of the leading-edge vortex. This pattern of vorticity is well-established and in accord with, for example, the laser Doppler anemometry measurements of Riley and Lowson[3] and the aforementioned imaging of Magness et al.[1]

Whereas the aforementioned investigations focused on wings having relatively high sweep angle, much less is known of the averaged flow structure on wings with moderate or low sweep angle. Ol and Gharib[4] compared the flow structure on wings having sweep angles of $\Lambda = 50$ and 65 deg, using a technique of stereo imaging. Based on patterns of averaged velocity and vorticity in the crossflow plane, they show that the wing of low sweep angle of $\Lambda = 50$ deg exhibits distinctive features, especially at a higher angle of attack, as a result of the earlier onset of vortex breakdown and a large-scale collapse of the rolled-up, leading-edge vortex structure. Gursul et al.[5] point out several interesting features of dye-visualized vortex cores

on wings of various planforms having relatively low sweepbreak angle.

B. Small-Scale Patterns of Flow Structure

The occurrence of small-scale vortical (subvortical) structures is well known. Their quantitative, time-averaged features have been assessed in detail by Riley and Lowson,[3] who undertook an extensive study, using laser Doppler anemometry, of the flow structure on a wing of sweep angle $\Lambda = 85$ deg. On the basis of averaged vorticity measurements, they revealed a system of steady, corotating, small-scale vortices. These substructures were observed in earlier investigations by Payne et al.,[6] Lowson,[7] and Reynolds and Abtahi[8] using visualization techniques and more recently by Washburn and Visser[9] and Mitchell et al.[10] via time-averaged measurements of the flow structure. Visbal and Gordnier[11] and Gordnier and Visbal[12] performed the first numerical simulations of the instantaneous structure on wings of relatively large and small sweep angle respectively. They demonstrated that steady substructures are apparent in the time-averaged (mean) patterns of the transitional turbulent shear layer from the leading edge.

In parallel with the investigation of the aforementioned steady substructures, Riley and Lowson[3] addressed time-dependent instabilities from the leading edge of a delta wing. These unstable structures were first observed by Gad-el-Hak and Blackwelder.[13] Recently, Ozgoren et al.[14] provided an additional perspective on this instability. Lowson,[7] using smoke visualization, characterized both this unsteady type of instability, as well as the aforementioned steady, subvortical instability, and noted that their coexistence could result in interaction and thereby interference between the two basic forms of instabilities. Lowson[7] indicates that the unsteady structures can coalesce, or merge, in a similar spirit as for the classical two-dimensional mixing layer addressed by Winant and Browand.[15] Gordnier and Visbal[16] performed the first computations of the unsteady substructures in the shear layer from the leading edge, and Gordnier and Visbal[17,18] further characterized features of the unsteady instability from the leading edge; it was coupled with unsteady boundary-layer separation from the leeward surface of the wing. Cipolla and Rockwell[19] demonstrated, via quantitative imaging, existence of small-scale structures consistent with the aforementioned simulations. Additional features of instabilities from the leading edge are addressed by Visbal and Gordnier[11] and Gordnier and Visbal.[12]

In a more general sense, several types of physical mechanisms can contribute to unsteadiness of the flow structure, at least for sufficiently large values of sweep angle. They include the helical mode instability of vortex breakdown, as characterized for an internal flow by Garg and Leibovich,[20] and flow past a delta wing of large sweep angle by Gursul,[21] as well as other mechanisms summarized and classified by Menke et al.[22] At lower values of sweep angle of attack, Gordnier and Visbal[12] have shown that pronounced unsteadiness can arise from periodic wandering of the vortex core, which is caused by a complex interaction of vortices from the leading edge and the leeward surface of the wing.

The possibility of controlling the unsteady structure on a delta wing by application of small amplitude perturbations has been addressed by Gad-el-Hak and Blackwelder,[23] who demonstrated the consequence of small-amplitude pulsations of flow through the edge of a delta wing on the instability. Ozgoren et al.[24] characterized the effect of perturbations of the entire wing on the time-averaged features of the multiple shear layer structure of the leading-edge vortex, including the onset of vortex breakdown.

C. Unresolved Issues

1. Averaged Structure of Shear Layer from Leading Edge of Wing

Of primary interest in recent years has been the structure of leading-edge vortices from slender wings of relatively high sweep angle. For the case of a wing with low sweep angle (less than 40 deg), the averaged, quantitative structure has received very little attention. The issue arises as to what degree a well-defined vortex core, in the form of a single-large-scale concentration of vorticity, can exist, particularly in regions where vortex breakdown and the onset of stall are prevalent, which is the focus of the present investigation. Correspondingly, the streamline topology and the possible existence and location of saddle points in the crossflow plane have not been pursued. At sufficiently high angle of attack, the manner in which this topology is altered, in relation to development of gross stall on the wing surface, remains unclarified. Such changes in the topological features are expected to influence the time-averaged forces and moments on the wing and thereby the steady-state performance characteristics.

2. Unsteady Features of Separated Layer Adjacent to Surface of Wing

It is anticipated that the vorticity layer adjacent to the surface of the wing will exhibit significant unsteadiness, especially when vortex breakdown/stall occur. The relationship between the patterns of fluctuating velocity amplitude and averaged vorticity over the crossflow plane has not been addressed for a wing of low sweep angle. These features are, of course, related to the instantaneous, whole-field patterns of discrete vortical structures and whether they retain their identity or give way to larger-scale clusters. This instantaneous structure, in turn, will be related to the spectral content of the velocity fluctuation(s) as a function of distance along the separated layer adjacent to the wing surface. These aspects have not been pursued. A knowledge of the successive, instantaneous states of the flow, and their assessment using spectral analysis techniques, can provide insight into the origin of unsteady buffet loading of the wing. This information could potentially be used in semi-empirical models that relate the flow structure above the wing to the unsteady pressure at its surface.

3. Control of Flow Structure by Leading-Edge Perturbations

The consequence of small-amplitude perturbations of the leading edge, at an appropriate frequency, on the time-averaged pattern of the separated shear layer adjacent to the wing surface, has not been addressed. The perturbation that yields the largest change in the flow pattern should be defined, in relation to the inherent formation frequency of vortical structures from the edge. An understanding of this type of control concept could yield practical techniques for controlling the forces and moments on a wing by alteration of the flow structure.

The aim of this investigation is to pursue these unresolved concepts by use of a technique of high-image-density PIV and appropriate processing of selected and cinema sequences of images.

II. Experimental System and Techniques

All experiments were undertaken in a large-scale water channel facility. Flow is pumped into a large settling tank and passes through a system of honeycomb and screen, followed by a 2:1 contraction that is connected to the main test section, which has a length of 4928 mm, a width of 927 mm, and a depth of 610 mm. The freestream turbulence intensity at the entrance to this test section is less than 0.1%.

The design of the delta wing was based on consideration of key elements of planforms representing unmanned combat air vehicles, which typically have a low-to-moderate values of sweep angle. Based on these considerations, the sweep angle of the wing was specified as $\Lambda = 38.7$ deg. The chord C was 101.6 mm, and the total span at the trailing edge was 254 mm. The thickness of the wing was 3 mm, and its leading edges were beveled on the windward side at an angle of 30 deg. For all experiments, the value of Reynolds number based on chord C was maintained at 10^3, which corresponded to a freestream velocity $U = 98.8$ mm/s. The wing was maintained in a nominally horizontal position by a slender support strut that extended vertically from the midchord of the wing. This strut had a width of 4 mm and a streamwise length of 35 mm. Assessment of this type of strut arrangement involved comparison with complementary experiments involving a nominally horizontal sting and comparison of the location of vortex breakdown for wings of different sweep angle. This strut arrangement had an insignificant effect on the flow structure on the leeward side of the wing.

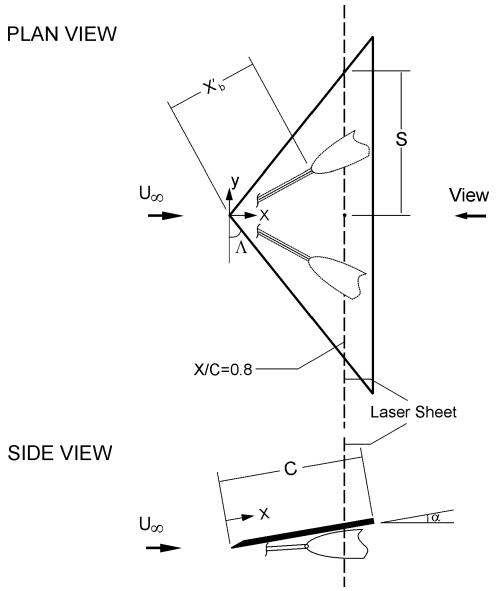

Fig. 1 Schematic of experimental arrangement showing delta wing, laser-sheet location, and definition of key parameters.

The present investigation focuses on global, instantaneous patterns of the flow structure, which are acquired in a cinema sequence using a technique of high-image-density PIV. This approach not only provides the sequence of instantaneous states of the flow structure but also serves as the basis for determination of time-averaged representations. The flow is seeded with 12-μm metallic-coated hollow plastic spheres, which are essentially neutrally buoyant. The seeding density of these particles was sufficiently large, such that the high-image-density criterion was satisfied. These particles were illuminated by a dual-pulsed Yag laser system, which has a maximum output of 90 mJ. To generate a laser sheet of desired thickness, focal distance, and orientation, the laser beam was transmitted through a system of cylindrical and spherical lenses. An overview of the laser-sheet location, relative to the delta wing, is provided in Fig. 1. For the present investigation, it was determined, on the basis of preliminary experiments, that the major features of the flow structure could best be determined at the streamwise location $x/C = 0.8$, and therefore this position of the laser sheet is employed in the present study. Furthermore, preliminary dye visualization, as well as initial PIV experiments, showed that the characteristic states of the flow structure were well represented by angles of attack $\alpha = 7$, 13, 17, and 25 deg, and therefore these values were employed for detailed imaging. This dye visualization indicates that the axis of the vortex was at an angle of 30 deg with respect to the plane of symmetry of the wing. The angle between the nominal axis of the vortex and the aforementioned plane of the laser sheet was therefore 60 deg, rather than an angle of 90 deg, which would correspond to perfect alignment of the axis of the vortex and the surface normal of the plane of the laser sheet. The patterns of flow topology characterized in the plane of the laser sheet must therefore be viewed as those on a skewed plane. This skew angle can alter the affected locations of certain critical points of the topology, relative to the locations deduced from viewing on a plane orthogonal to the axis of the vortex. A further aspect of the field of view corresponding to the plane of the laser sheet is that the flow structures was characterized over half the wing, rather than the entire spanwise extent of the wing, in order to maximize spatial resolution of the measurements. As a consequence, it is not possible to monitor time-dependent variations of the processes of vortex breakdown and stall on opposing sides of the wing.

Images were acquired at a framing rate of 15 frames per second, thereby providing a cinema series of instantaneous images. These images were recorded on a high-resolution camera having an array of 1024×1024 pixels. Because the characteristic frequencies of the unsteady events were significantly smaller than the framing rate, it is possible to perform autospectral and cross-spectral analysis of the flow structure at a large number of points over the plane of the imaging, thereby yielding averaged spectral representations, all of which are based on the same time record.

Patterns of instantaneous velocity vectors were calculated using a cross-correlation technique between successive patterns of particle images, which resulted from illumination by the dual-pulsed laser system. In essence, two interrogation windows were employed: 32×32 pixels and 16×16 pixels, referred to as low- and high-resolution cases herein. For both windows, an effective overlap of 50% was used, in order to satisfy the Nyquist criterion. This approach resulted in effective grid sizes of 2.62 mm in the plane of the laser sheet. The minimum number of particle images contained within a given window boundary was 15 to 20, respectively, thereby exceeding the criterion for high image density.

III. Dye Visualization

Representative dye visualization is shown in Fig. 2 for the case of the stationary wing at three values of angle of attack α. At the lowest two values of $\alpha = 7$ and 13 deg, dye was injected from two localized ports on the windward surface located close to the apex of the wing. At $\alpha = 7$ deg, the apparent centerlines of the leading-edge vortices are designated, and it is clear that initial disruptions of the marker can occur, at locations of the order of 0.3 to $0.5C$, in which C is the chord of the wing. At locations sufficiently far downstream, at $x/C = 0.6$ to 0.8, a large-scale widening of the marker occurs. This two-stage process of vortex breakdown, that is, an initial disruption, then a large-scale widening, has a form remarkably similar to the computations of Gordnier and Visbal for a wing of low sweep angle $\Lambda = 50$ deg. This overall pattern of vortex breakdown therefore appears to be an inherent feature of the flow structure on wings of low sweep angle.

At $\alpha = 13$ deg, the streamwise extent of the organized portion of the dye marker emanating from the apex is very short. The central portion of the wing is unmarked by dye because it is continuously swept downstream past the trailing edge. On the other hand, the regions of the wing outboard of this central portion show a low velocity region of dye adjacent to the surface.

At 17 deg, the entire wing is filled with a region of low-velocity dye, as shown in Fig. 2c. In presence of an applied, small-amplitude perturbation, shown in Fig. 2d, the flow structure of the visualized pattern at $\alpha = 17$ deg resembles, in a general sense, the structure at $\alpha = 13$ deg on the stationary wing.

Taken together, the foregoing visualizations suggest overall features of the flow patterns, which are addressed herein using quantitative imaging of the instantaneous and averaged flow structure.

IV. Averaged Velocity and Streamline Topology

Figure 3 shows patterns of time-averaged velocity $\langle V \rangle$ and streamlines $\langle \Psi \rangle$ corresponding to the flow structure at $x = 0.8C$. In this and subsequent figures, the semispan S corresponds to the local value of S at a given value of dimensionless chordwise distance s/C; it does not have a single value corresponding to the value of the semispan at the trailing-edge $x/C = 1$. In Fig. 3 and subsequent figures, the fact that only a fraction of the local semispan S is shown arises from the variable zoom during image acquisition. Comparison with the dye-visualization image of Fig. 2 shows that the chordwise location $x/C = 0.8$ lies within the region. In Fig. 3 and subsequent figures, the fact that only a fraction of the local semispan S is shown arises from the variable zoom during image acquisition.

Comparison with the dye-visualization image of Fig. 2 shows that the chordwise location $x/C = 0.8$ lies within the region of significant disruption of the dye marker at $\alpha = 7$ deg and is well downstream of the substantial widening of the dye marker at $\alpha = 13$ deg. At $\alpha = 17$ and 25 deg (not shown), dye simply floods the surface of the wing, which suggests that the region near the surface flow pattern on the wing is fully stalled. Remarkably, however, all of the patterns of Fig. 3 show a definable time-averaged structure.

At $\alpha = 7$–17 deg an identifiable interface exists between a region of high velocity flow below the wing and very low velocity immediately adjacent to the wing. In other words, at this interface this velocity field is characteristic of a separated free-shear layer. At

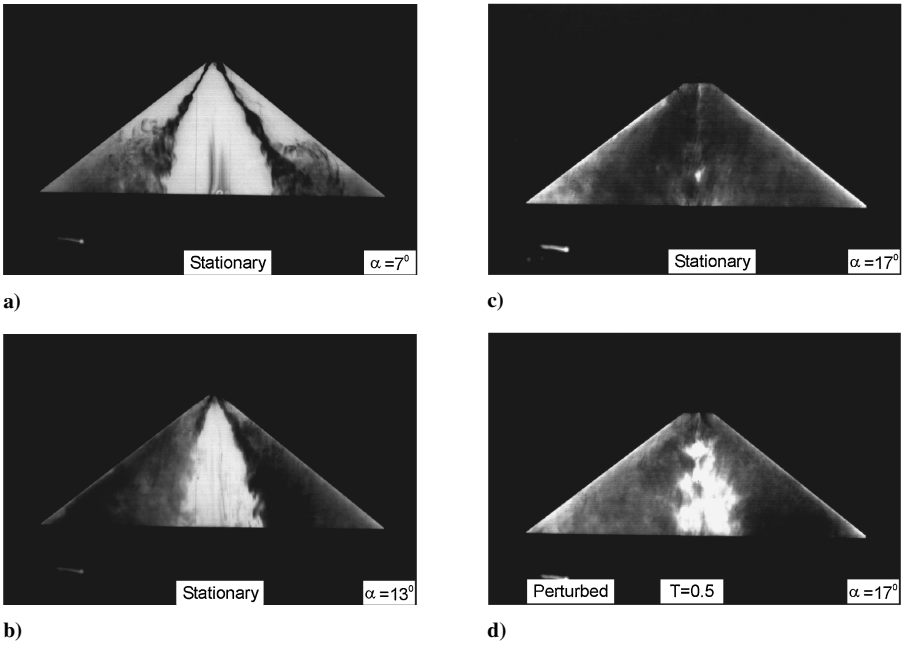

Fig. 2 Dye visualization at three representative angles of attack. For images $\alpha = 7$ and 13 deg, dye is injected through two discrete ports at the apex of the wing, whereas at $\alpha = 17$ deg, dye is injected along the leading edge on the windward side of the wing. For the perturbed wing, the perturbation amplitude and period are $\alpha_0 = 1$ deg and $T = 0.5$ s.

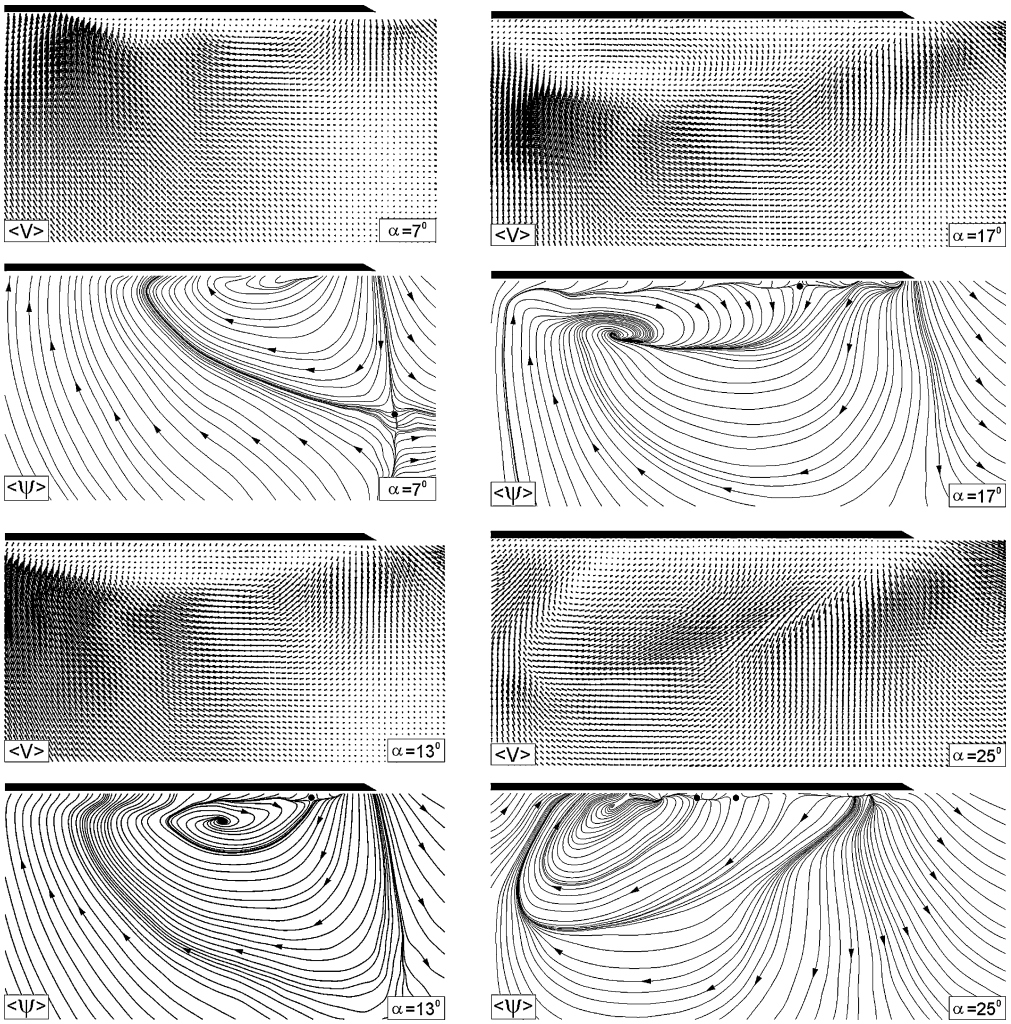

Fig. 3 Patterns of averaged velocity $\langle V \rangle$ and streamline $\langle \Psi \rangle$ topology at four values of angle of attack $\alpha = 7$, 13, 17, and 25 deg. Laser sheet is located at $x/C = 0.8$. Spanwise extent of wing corresponds to 0.82 S at $\alpha = 7$ and 13 deg and 0.94 S at $\alpha = 17$ and 25 deg, in which S is the semispan of the delta wing at the location of the laser sheet $x/C = 0.8$.

$\alpha = 25$ deg, the interface region has a different form, and the spatial extent of the very low velocity region is confined to a domain very close to the surface of the wing. Unlike cases at low angle of attack, the interface does not correspond to an abrupt decrease of velocity between the exterior flow and the region of flow closer to the wing. Rather, the magnitude of velocity is of the same order on either side of the interface.

The corresponding streamline topology, which is constructed from these averaged velocity fields, indicates a saddle point at $\alpha = 7$ deg, which is designated by a circular dot. It appears well below and slightly outboard of the leading edge of the wing. Furthermore, the streamline pattern inside the major streamlines that connect to the saddle point does not exhibit a well-defined swirl pattern. All of these features of the streamline topology are distinctly different from those associated with wings having relatively high sweep angle, as characterized by Magness et al.[1]

At $\alpha = 13$ deg, the aforementioned saddle point has been displaced downward and lies outside of the field of view. A well-defined swirl pattern exists. It does not emanate, however, from the leading edge of the wing. Rather, it appears to originate from a saddle point located at the position of the black dot. This displacement from the leading edge of the wing is caused by the extensively separated flow, evident by comparison with the dye visualization at $\alpha = 13$ deg in Fig. 2. A similar saddle point, which is displaced inboard from the leading edge, is indicated by the black dot in the streamline topology at $\alpha = 17$ deg. Finally, at $\alpha = 25$ deg an identifiable swirl pattern is barely evident, and the entire streamline topology takes on an unconventional form, as a result of the highly stalled flow over the surface of the wing.

V. Patterns of Averaged Vorticity and Fluctuating Velocity

In Fig. 4, patterns of time-averaged vorticity $\langle\omega\rangle$ are compared with the rms of the transverse (vertical) velocity fluctuation $w_{\rm rms}$ normalized by the freestream velocity U, that is, $w_{\rm rms}/U$, as well as

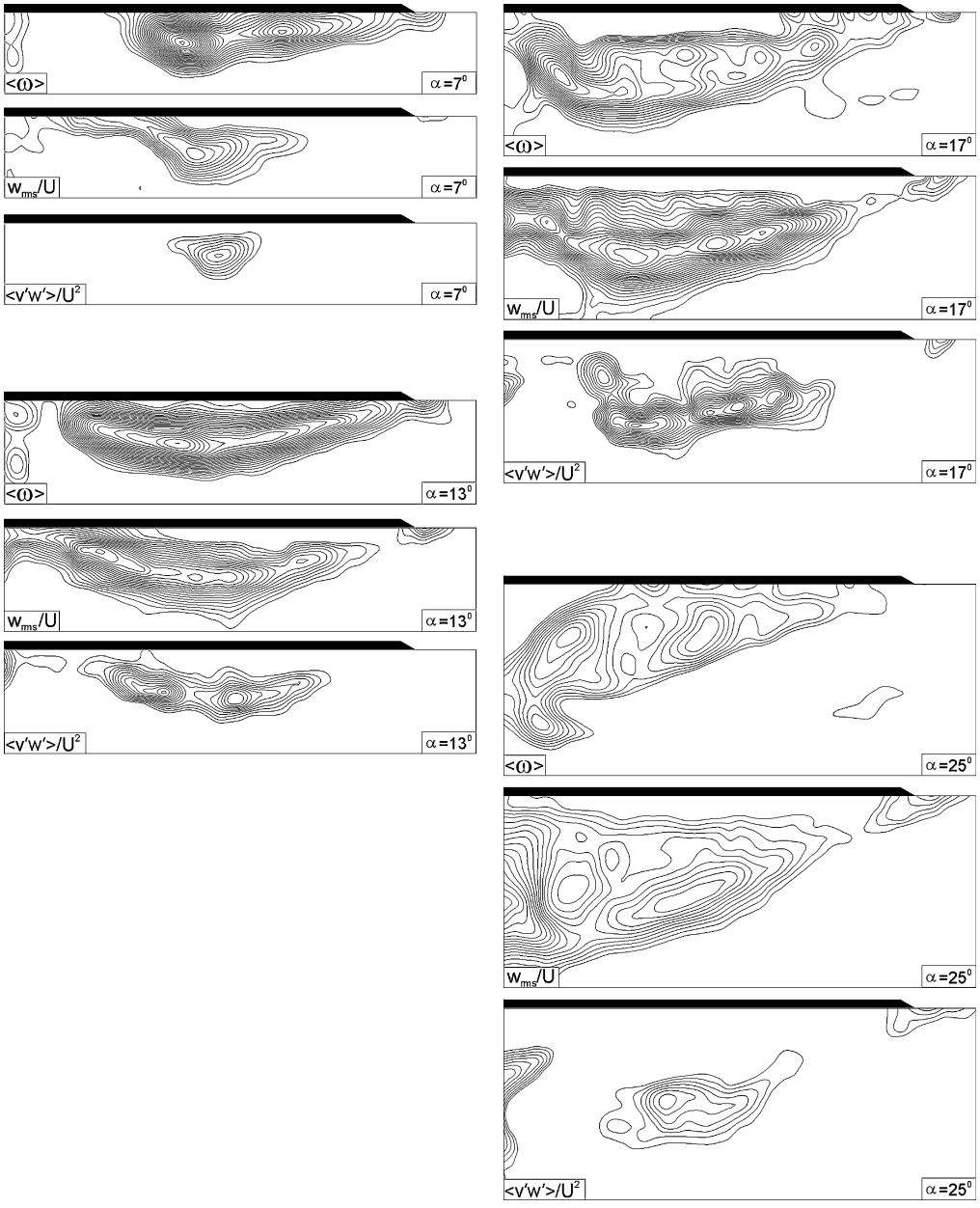

Fig. 4 Patterns of averaged vorticity $\langle\omega\rangle$, contours of constant vertical (transverse) velocity fluctuation $w_{\rm rms}/U$, and Reynolds-stress correlation $\langle v'w'\rangle/U^2$. Angles of attack are $\alpha = 7$, 13, 17, and 25 deg. Laser sheet is located at $x/C = 0.8$. For contours of averaged vorticity, minimum and incremental values are $[\langle\omega\rangle]_{\rm min} = -0.3\ {\rm s}^{-1}$ and $\Delta[\langle\omega\rangle] = -0.15\ {\rm s}^{-1}$. For contours of constant velocity fluctuation, $[w_{\rm rms}/U]_{\rm min} = 0.025$, and $\Delta[w_{\rm rms}/U] = 0.005$. For contours of constant Reynolds-stress correlation, $[\langle v'w'\rangle/U^2]_{\rm min} = -0.0004$, and $\Delta[\langle v'w'\rangle/U^2] = -0.0002$. Spanwise extent of wing corresponds to 1.0 S, in which S is the semispan of the delta wing at the location of the laser sheet $x/C = 0.8$.

with the Reynolds-stress correlation $\langle v'w' \rangle / U^2$, for angles of attack $\alpha = 7$, 13, 17, and 25 deg.

To allow direct comparison, the minimum and incremental values of all contour patterns of averaged vorticity $\langle \omega \rangle$ in Fig. 4 are maintained the same at all values of $\alpha = 7$, 13, 17, and 25 deg. Similarly, the same minimum and incremental values are maintained for the contours of w_{rms}/U and $\langle v'w' \rangle / U^2$.

Consider, first, the patterns of averaged vorticity $\langle \omega \rangle$ at $\alpha = 7$ and 13 deg. They take the form of an elongated layer with one or two vorticity extrema. Comparison with Fig. 3 shows that, along each of these layers, the maximum value of vorticity $\langle \omega \rangle$ corresponds to the interface between regions of high and low velocity in the corresponding plots of averaged velocity $\langle V \rangle$ at $\alpha = 7$ and 13 deg. That is, the elongated layers are characteristic of a free-shear layer as viewed in this crossflow plane. Furthermore, the pattern of $\langle \omega \rangle$ at $\alpha = 17$ deg in Fig. 4 has a generally similar form, but the loci of maximum vorticity are at a less well-defined interface between higher and lower velocities. It is evident that, however, at this larger angle of attack the peak value of vorticity is not as large as at $\alpha = 7$ and 13 deg. Finally, at the largest angle of attack $\alpha = 25$ deg, the form of the vorticity pattern $\langle \omega \rangle$ is fundamentally different. The elongated region of vorticity no longer appears to emanate from the leading edge of the wing. Furthermore, the peak values of vorticity no longer occur at the interface referred to in the pattern of $\langle V \rangle$ at $\alpha = 25$ deg in Fig. 3. Remarkably, the peak values of vorticity are further reduced from those at $\alpha = 17$ deg.

It is appropriate to compare the elongated layers of vorticity $\langle \omega \rangle$ at, for example, $\alpha = 7$ and 13 deg in Fig. 4, with the corresponding patterns of streamline topology in Fig. 3. The location of an extremum of vorticity is not always coincident with the focus (apparent center) of the streamline pattern, and, furthermore, the spatial extent of the large-scale swirl pattern of streamlines is substantially larger than the thickness of the elongated vorticity layer. These observations are apparently caused by the very rapidly distorting flow that separates from the leading edge of the wing and, in fact, directly analogous patterns of averaged vorticity and streamline topology, including the lack of precise correspondence between them, that have been observed in the very near wake of a cylinder, where the plane of observation is orthogonal to the axis of the separating shear layer. As shown, for example, by Akilli and Rockwell,[25] an elongated vorticity layer, which does not culminate in a single, large-scale vortical structure, is nevertheless associated with a pattern of streamline topology having a well-defined swirl pattern with a focus.

The aforementioned values of vorticity $\langle \omega \rangle$ are related to the normalized component of vertical velocity fluctuation w_{rms}/U, at least for the lower values of angle of attack $\alpha = 7$, 13, and 17 deg. For these values of α, the locations of maximum values of w_{rms}/U can be tracked as a function of spanwise distance along each elongated pattern of w_{rms}/U. These maxima generally follow the peak values of $\langle \omega \rangle$. That is, the largest velocity fluctuations occur in the region of maximum vorticity and thereby at the interfaces in the patterns of $\langle V \rangle$ shown in Fig. 3.

In turn, the patterns of velocity fluctuation w_{rms}/U are associated with the Reynolds-stress correlation $\langle v'w' \rangle / U^2$, that is, with the degree of turbulence production in the free-shear flow, at least at angles of attack $\alpha = 7$, 13, and 17 deg. The largest values of $\langle v'w' \rangle / U^2$ tend to occur approximately at half the semispan S, that is, at 0.5 S for all values of angle of attack $\alpha = 7$–17 deg. The loci of extrema of the correlation $\langle v'w' \rangle / U^2$ are generally in accord with the maxima of w_{rms}/U. In fact, the peak magnitude of the correlation $\langle v'w' \rangle / U^2$ increases with angle of attack $\alpha = 7$–17 deg.

At the highest angle of attack $\alpha = 25$ deg, the patterns have a fundamentally different form. The pattern of w_{rms}/U is substantially broader than at lower angle of attack, and, moreover, the peak value is substantially lower than at $\alpha = 17$ deg. Regarding the corresponding Reynolds-stress correlation $\langle v'w' \rangle / U^2$, its value is substantially lower than at $\alpha = 17$ deg. This remarkable attenuation of the fluctuating velocity magnitude, and the corresponding Reynolds-stress correlation is associated with the radical change of the pattern of velocity $\langle V \rangle$ and streamline $\langle \Psi \rangle$ topology shown at $\alpha = 25$ deg in Fig. 3. In essence, the loss of identity of the shear-layer interface and the elongated vorticity layer emanating from the leading edge of the wing, which are present at lower angle of attack $\alpha = 7$–17 deg, yield a substantial reduction in the magnitude of the fluctuating velocity field.

VI. Instantaneous Patterns of Vorticity

The patterns of velocity fluctuation w_{rms}/U and Reynolds-stress correlation $\langle v'w' \rangle / U^2$ described in Sec. V are intimately related to the patterns of instantaneous vorticity and their evolution with time. Figure 5 shows two randomly selected patterns of instantaneous vorticity at each angle of attack $\alpha = 7$–25 deg. At $\alpha = 7$ deg, the individual vorticity concentrations retain their identity along the surface of the wing. That is, interaction between concentrations is not evident. This pattern is also evident in Fig. 4, in a smoothed version, as a result of the effects of time-averaging of fluctuations, or jitter, of the instantaneous locations of the vorticity concentrations. It is remarkably similar to that on a wing of low sweep angle ($\Lambda = 50$ deg) at low angle of attack ($\alpha = 5$ deg) computed by Gordnier and Visbal.[12] In Fig. 5, at $\alpha = 7$ deg the typical wavelength between these concentrations is $\lambda/S = 0.25$, in which S is the semispan of the wing at the chordwise location of interest herein, $x/C = 0.8$. On the other hand, at $\alpha = 13$ deg, smaller-scale vorticity concentrations, with a smaller wavelength $\lambda/S = 0.15$ are formed immediately after separation from the leading edge of the wing. Note that these concentrations do not form directly from the edge, but are initially identifiable along the surface of the wing inboard of the edge. In fact, this feature is even more prevalent at high values of $\alpha = 17$ and 25 deg. Farther inboard, larger-scale clusters of vorticity appear. At $\alpha = 17$ deg, the initially formed concentrations also have a relatively small wavelength, which is not as clearly defined as at lower α. The change in the patterns of instantaneous vorticity ω at successive values of $\alpha = 7$, 13, and 17 deg is associated with a substantial increase in both velocity fluctuation amplitude w_{rms}/U and Reynolds-stress correlation $\langle v'w' \rangle / U^2$, which is evident from cross comparison of the images at $\alpha = 7$, 13, and 17 deg in Fig. 4.

On the other hand, at the highest angle of attack $\alpha = 25$ deg defined clusters of vorticity are first detectable at a significant distance inboard from the leading edge. Such patterns are associated with relatively low values of the Reynolds-stress correlation $\langle v'w' \rangle / U^2$ and velocity fluctuation w_{rms}/U, evident at $\alpha = 25$ deg in the images of Fig. 4. The occurrence of large-scale stall at $\alpha = 25$ deg therefore results in a reduction in level of the unsteadiness, relative to lower values of α where a well-defined separated shear layer, that is, vorticity layer, is located adjacent to the surface of the wing.

VII. Spectra Along Separated Vorticity Layer

As shown in Fig. 4, the elongated vorticity layers from the leading edge are associated with corresponding patterns of vertical velocity fluctuation amplitude w_{rms}/U, and at lower values of angle of attack α the peak values of w_{rms}/U follow the peak values of averaged vorticity $\langle \omega \rangle$. In Fig. 6, for each value of angle of attack α spectra of the transverse (vertical) velocity fluctuation were evaluated at successive locations along the locus of maximum w_{rms}/U. These locations are indicated by the solid black points on each of the patterns of w_{rms}/U for angles of attack $\alpha = 7$, 13, 17, and 25 deg.

At $\alpha = 7$ deg, the frequency f_0 of the spectral peak is at $f_0 = 3.4$ Hz, and the largest amplitude of this spectral peak occurs at the maximum of w_{rms}/U, which is well inboard of the leading edge. Then, as the surface of the wing is approached this peak is rapidly attenuated, and barely detectable. The form of these spectra is directly related to the patterns of instantaneous vorticity concentrations, as shown at $\alpha = 7$ deg in Fig. 5.

At $\alpha = 13$ deg, the spectral peak closest to the leading edge, which is relatively broad, is initially centered at $f_0 = 4.6$ Hz. For increasing distance along the vorticity layer, peaks at lower values of f_0 are evident; they lie in the range $2.4 \leq f_0 \leq 3.2$ Hz. This lowering of the peak frequency f_0 is consistent with the occurrence of larger-scale vortical structures shown at $\alpha = 13$ deg in Fig. 5.

Similarly, at $\alpha = 17$ deg the initial, broad spectral peak has a relatively high center frequency $f_0 = 4.1$ Hz. Farther along the layer, two peaks are evident at $f_0 = 2.1$ and 3.2 Hz, and, finally, a relatively low-frequency component is apparent at $f_0 = 0.5$ Hz, as the shear

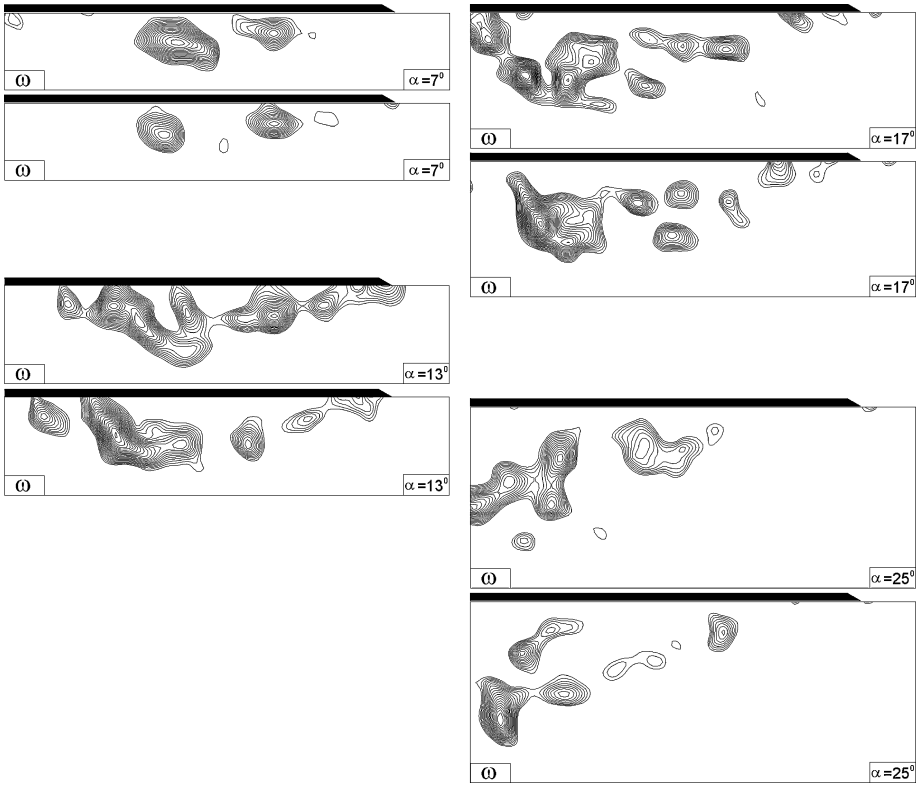

Fig. 5 Patterns of instantaneous vorticity ω at two randomly selected instants from a cinema sequence. Angles of attack are $\alpha = 7$, 13, 17, and 25 deg. Minimum and incremental values are $\omega_{min} = -1.5\ s^{-1}$ and $\Delta\omega = -0.25\ s^{-1}$. Spanwise extent of wing corresponds to 1.0 S, in which S is the semispan of the delta wing at the location of the laser sheet $x/C = 0.8$.

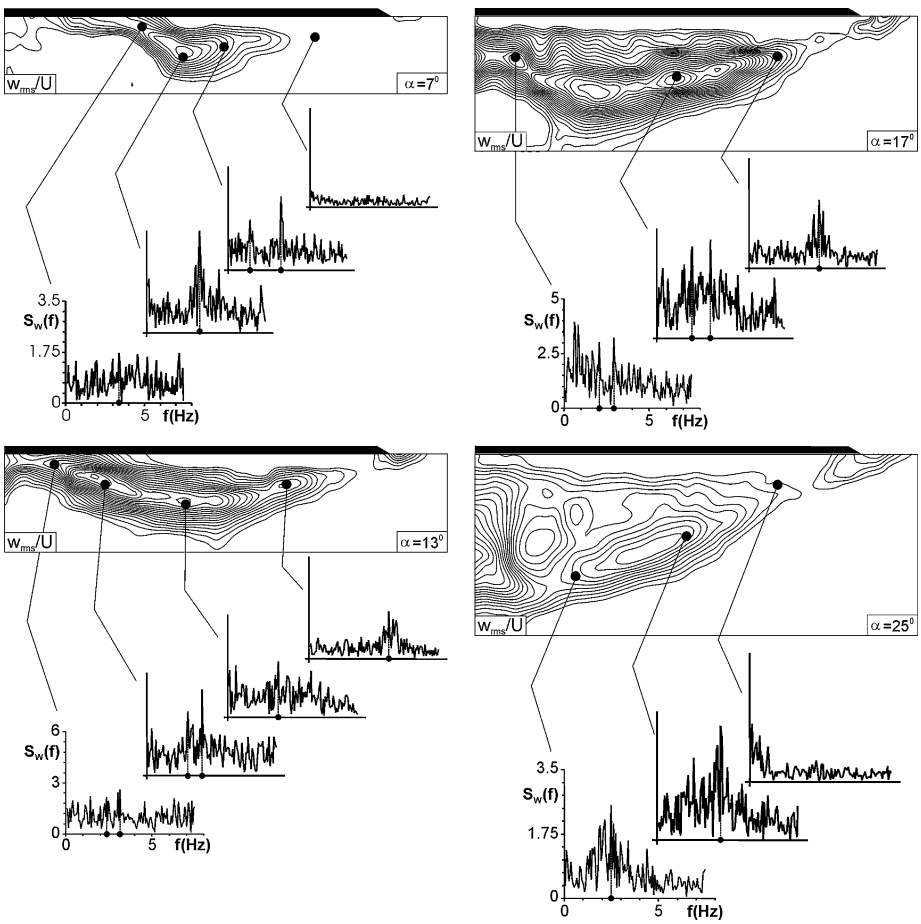

Fig. 6 Spectra S_w of velocity fluctuation at selected locations in separated shear layer. Each spectrum is referenced to the indicated location in the pattern of constant contours of w_{rms}/U. Parameters for these contour levels are given in Fig. 4. Spanwise extent of wing corresponds to 1.0 S, in which S is the semispan of the delta wing at the location of the laser sheet $x/C = 0.8$.

layer approaches the surface of the wing. This successive lowering of the values of f_0 is again associated with the occurrence of larger-scale vortical structures along the shear layer.

At the highest angle of attack $\alpha = 25$ deg, a reasonably defined, somewhat broadband peak is detectable at a location well inboard of the leading edge. This predominant peak is centered at $f_0 = 3.4$ Hz and moves to a lower value of $f_0 = 2.5$ Hz farther along the layer. At this high angle of attack, it is apparent that the occurrence of larger-scale vortical structures along the separated vorticity layer still plays a role in shifting the broadly defined peak at f_0 to lower frequencies.

Viewing the patterns of spectra at all values of α in Fig. 6, it is evident that, at the smallest angles of attack $\alpha = 7$ and 13 deg, the eventual reattachment of the shear layer to the surface of the wing, evident in patterns of averaged velocity of Fig. 3 and vorticity of Fig. 4, is associated with attenuation of the predominant spectral peak. At a sufficiently high angle of attack $\alpha = 17$ deg, this tendency toward reattachment is associated with the appearance of a very low frequency. At $\alpha = 25$ deg, such reattachment does not occur, and a defined, but relatively broadband, peak persists.

The dimensionless frequencies of the spectral peaks at f_0 can be expressed as $f_0 C/U$. For the spectra of Fig. 6, the identifiable spectral peaks in the early stages of development of the shear layer are in the range $3.3 \le f_0 \le 4.6$ Hz, which correspond to $3.39 \le f_0 C/U \le 4.73$. Farther along the separated layer, where larger-scale clusters of vorticity occur, the range of values is lower, that is, 0.5 Hz $\le f_0 \le 3.2$, which correspond to $0.51 \le f_0 C/U \le 3.29$. This range of $f_0 C/U$ is remarkably similar to the band of identifiable frequencies in a spectrum computed by Gordnier and Visbal[12] in the region downstream of vortex breakdown on a wing of low sweep angle $\Lambda = 50$ deg.

As indicated in the citations in Sec. I, several physical mechanisms can contribute to unsteadiness of the flow structure on a delta wing. Menke et al.,[22] as well as works of Gursul cited therein, provide a classification of types of unsteadiness for wings having relatively large values of sweep angle $\Lambda = 65$ to 75 deg. Most relevant to our present considerations is the occurrence of 1) vortex shedding, typically when the vortex breakdown location reaches the apex of the wing ($0.25 \le f_0 C/U \le 0.6$); 2) unsteadiness associated with the helical mode of instability of vortex breakdown ($1.0 \le f_0 C/U \le 4$); and 3) the small-scale Kelvin–Helmholtz instability of the shear layer separating from the leading edge of the wing ($6 \le f_0 C/U \le 30$). For a wing having a relatively low sweep angle, for example, $\Lambda = 38.7$ deg of the present study, this type of detailed classification is not available.

As indicated in the foregoing images, a classical vortex core, marked by an approximately circular region of vorticity, does not exist in the images of the vorticity layer formed from the leading edge. It is therefore questionable that one can speak of a helical mode instability of vortex breakdown on wings of such low sweep. In fact, for the wing of relatively low sweep angle $\Lambda = 38.7$ deg investigated herein, it is apparent from the dye visualization at, for example, $\alpha = 7$ deg in Fig. 2, that a well-defined spiral, or bubble mode of vortex breakdown, does not occur. For all values of α considered herein, the crossflow planes lie within regions of vortex breakdown and stall, and maximum amplitudes of the spectra occur well inboard of the leading edge. For the present purposes, vortex

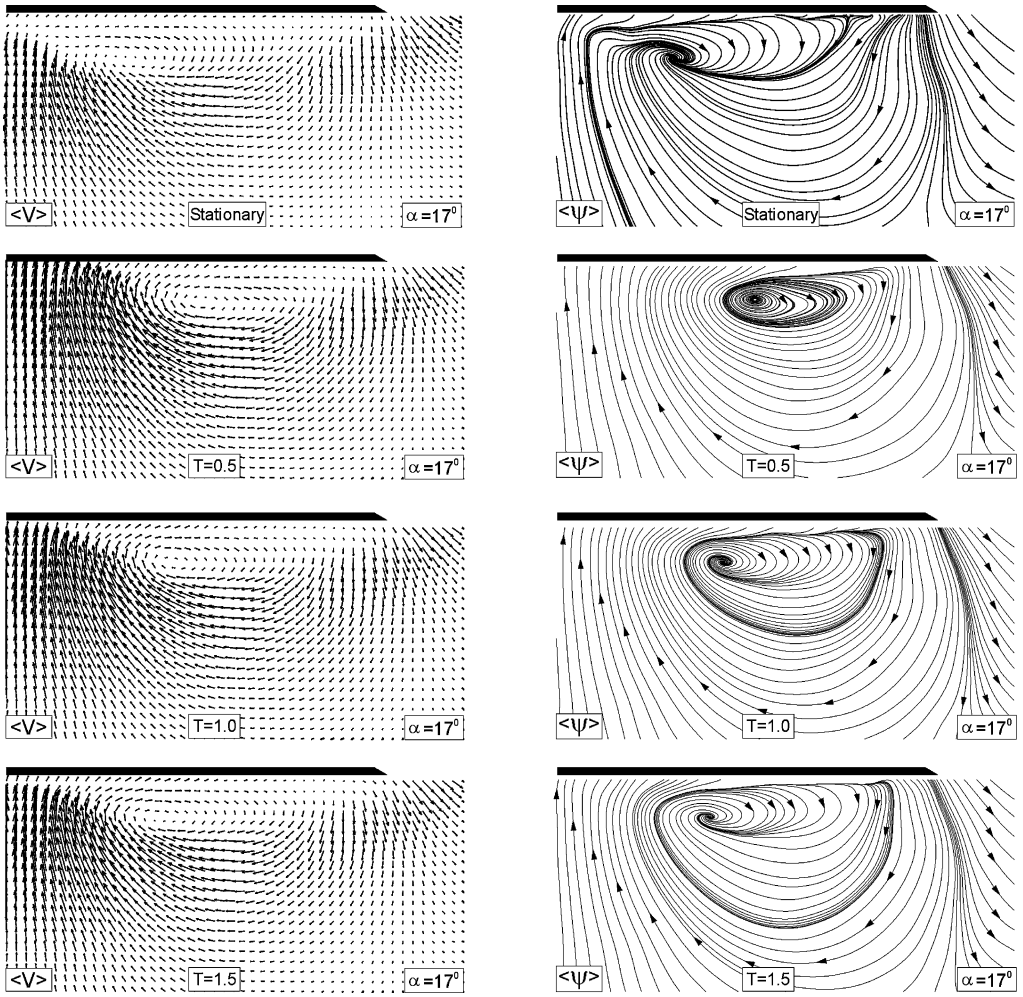

Fig. 7 Effect of small perturbations of wing on time-averaged patterns of velocity $\langle V \rangle$ and streamlines $\langle \Psi \rangle$, relative to the case of he stationary wing. Perturbation amplitude is $\alpha_0 = 1$ deg, and mean angle of attack is $\bar{\alpha} = 17$ deg. Perturbation is applied according to $\alpha(t) = \bar{\alpha} + \alpha_0 \sin(2\pi t/T)$. Values of perturbation period T are $T = 0.5$, 1.0, and 1.5 s. Spanwise extent of wing corresponds to 1.0 S, in which S is the semispan of the delta wing at the location of the laser sheet $x/C = 0.8$.

breakdown is simply defined as a severe disruption of the core of the vortex, as evident in the dye visualization of Fig. 2 at $\alpha = 7$ deg. This type of apparent breakdown might be associated with either jitter of the nominally stationary vortical substructures or unsteadiness associated with the fundamental or subharmonics of the inherent instability of the shear layer separating from the leading edge.

VIII. Effect of Controlled Perturbations on Averaged and Instantaneous Structure

Preliminary experiments indicated that at sufficiently high angle of attack, that is, $\alpha = 17$ deg, the flow structure was particularly sensitive to small-amplitude perturbations. On this basis, the delta wing was subjected to perturbations about its midchord. The amplitude $\Delta\alpha$ of these perturbations was kept small at $\Delta\alpha = 1$ deg, while the period T of the perturbation was varied. The smallest period of oscillation was $T = 0.5$, that is, $f = 2$ Hz, which lies in the lower range of frequency $0.5 \leq f_0 \leq 3.15$ of the self-excited instability, shown in the spectra of Fig. 6. In fact, this value of the perturbation period corresponds to the frequency range of the coalesced, or merged, small-scale vortical structures indicated at $\alpha = 17$ deg in Fig. 5. More specifically, $T = 0.5$ corresponds to the subharmonic of the highest frequency $f_0 \cong 4$ Hz in the initial region of the shear layer, as shown in Fig. 6. In addition, larger values of $T = 1.0$, 1.5, and 2.0 s were applied, with $T = 2.0$ corresponding to $f = 0.5$ Hz, which is the lowest low frequency in the spectrum at the location farthest from the leading edge along the vorticity layer, as shown in Fig. 6.

Patterns of time-averaged velocity $\langle V \rangle$ and $\langle \Psi \rangle$ are shown in Fig. 7. It is evident that the streamline topology undergoes a fundamental transformation, relative to the topology on the stationary wing, evident by comparison of the top two images of Fig. 7. That is, the topology is characteristic of a typical leading-edge vortex, and, in fact, comparison with the topology at $\alpha = 13$ deg for the stationary wing in Fig. 3, shows a close similarity to the pattern of $T = 0.5$ in Fig. 7. As the period of excitation is increased to values of $T = 1.0$ and 1.5, the topology relaxes toward that of the stationary wing, that is, the center of the spiral streamline pattern moves farther inboard and becomes less defined.

These changes in the patterns of velocity $\langle V \rangle$ and the streamline $\langle \Psi \rangle$ topology are associated with corresponding alterations of the patterns of averaged vorticity $\langle \omega \rangle$, velocity fluctuation amplitude $w_{\rm rms}/U$, and Reynolds stress $\langle v'w' \rangle / U^2$, as indicated in Fig. 8.

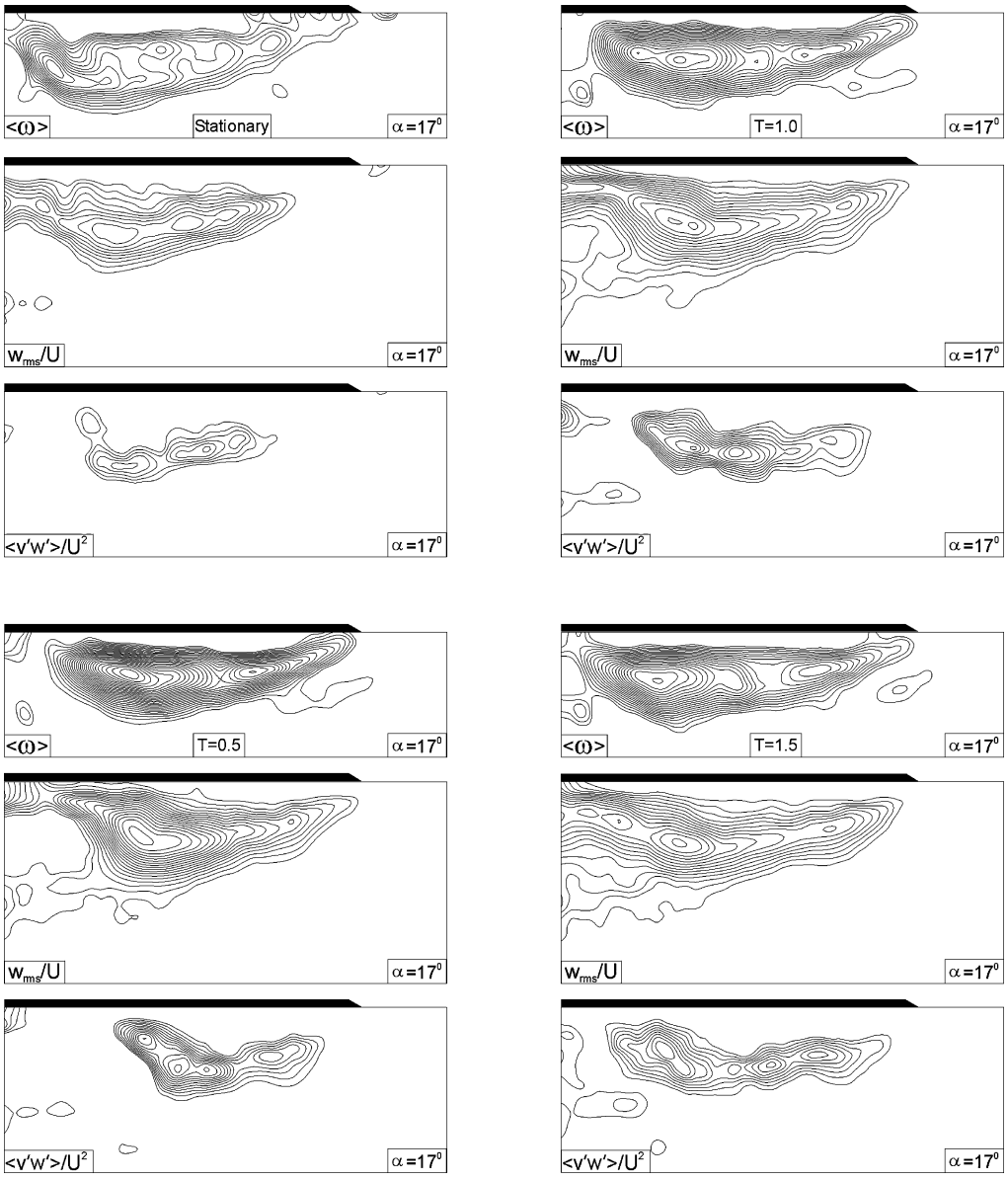

Fig. 8 Consequence of small-amplitude perturbation on patterns of averaged vorticity $\langle \omega \rangle$, rms of vertical (transverse) velocity fluctuation $w_{\rm rms}/U$, and Reynolds stress correlation $\langle v'w' \rangle / U^2$. For patterns of vorticity, $\langle \omega \rangle_{\rm min} = -0.4\ {\rm s}^{-1}$ and $\Delta[\langle \omega \rangle] = -0.2\ {\rm s}^{-1}$. For contours of constant $w_{\rm rms}/U$, $[w_{\rm rms}/U]_{\rm min} = 0.04$, and $\Delta[w_{\rm rms}/U] = 0.01$. For contours of constant Reynolds-stress correlation, $[\langle v'w' \rangle / U^2]_{\rm min} = -0.001$, and $\Delta[\langle v'w' \rangle / U^2] = -0.0005$. Spanwise extent of wing corresponds to 1.0 S, in which S is the semispan of the delta wing at the location of the laser sheet $x/C = 0.8$.

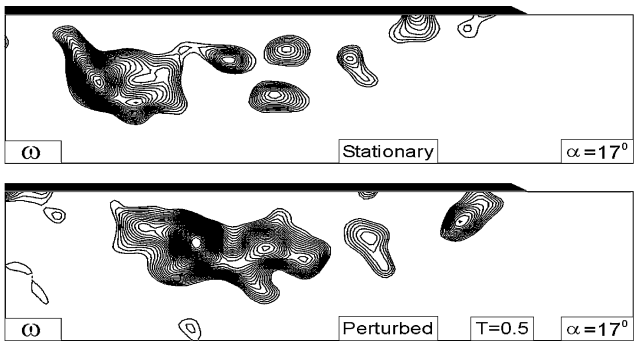

Fig. 9 Comparison of representative patterns of instantaneous vorticity ω for the stationary wing and the wing subjected to small-amplitude perturbations according to $\alpha(t) = \bar{\alpha}$ sine(ωt) in which $\bar{\alpha}$ 17 deg, $\alpha_0 = 1$ deg, and $\omega = 2\pi t/T$. Minimum and incremental values of vorticity are $\omega_{\min} = -1.5\ s^{-1}$ and $\Delta\omega = -0.25\ s^{-1}$. Spanwise extent of wing corresponds to 1.0 S, in which S is the semispan of the delta wing at the location of the laser sheet $x/C = 0.8$.

Comparing, first, the patterns of $\langle\omega\rangle$, it is evident that the perturbation at $T = 0.5$ results in a radically increased level of peak $\langle\omega\rangle$, as well as an increase in the degree of organization of the distribution of $\langle\omega\rangle$, relative to the pattern of $\langle\omega\rangle$ for the stationary wing. At larger values of perturbation period $T = 1.0$ and 1.5, this peak vorticity level decreases, and the ordered nature of the pattern is less apparent.

The increase in level of averaged vorticity $\langle\omega\rangle$ at $T = 0.5$ is accompanied by a substantial increase in the peak values of the velocity fluctuation in w_{rms}/U and Reynolds-stress correlation $\langle v'w'\rangle/U^2$, relative to the case of the stationary wing. At the highest value $T = 1.5$, these peak values have decreased significantly, relative to those at $T = 0.5$.

The patterns of instantaneous vorticity associated with the perturbation at $T = 0.5$ are shown in Fig. 9. It is evident that in presence of the perturbation a relatively large-scale cluster of vorticity is formed, as a result of the coalescence of a number of small-scale concentrations of vorticity. This larger-scale vorticity cluster forms closer to the leading edge of the wing than the cluster on the stationary wing. The physical mechanism for enhancement of the averaged structure described in the foregoing therefore involves more rapid development of patterns of coalesced vorticity.

IX. Conclusions

The flow structure on a delta wing of low sweep angle exhibits a number of distinctive characteristics, relative to the extensively investigated case of a slender, highly swept delta wing. Emphasis in the present investigation has been on crossflow planes, where vortex breakdown and stall phenomena occur; these phenomena are known to be important origins of unsteady buffet loading of the wing. The primary features of the flow structure, and the potential for their control, are summarized in the following:

1) The time-averaged flow structure shows a number of distinctive features relative to the structure on wings of relatively high sweep angle. Patterns of averaged velocity show a relatively narrow elongated region of low velocity immediately adjacent to the surface of the wing, which is bounded by a higher speed region. The interface between these two domains of the velocity field represents a region of high shear, and thereby the locus of unsteady events. The corresponding streamline topology exhibits a saddle point that is located outboard of the leading edge of the wing. At sufficiently high angle of attack, the separation streamline from the leading edge loses its identity. Patterns of averaged vorticity show an elongated layer parallel to the surface of the wing at sufficiently low angle of attack, a well-defined, dual-vortex substructure system is established. The aforementioned patterns of vortical structures and stall are expected to be a function of Reynolds number. Separation of the shear layer from the leading edge will be influenced by the existence of small-scale Kelvin–Helmholtz instabilities, of varying scale and circulation, as the Reynolds number is altered. Furthermore, the onset of stall from the surface of the wing can also be a function of Reynolds number. These issues await further investigation.

2) Unsteadiness of the flow structure is represented by patterns of rms velocity fluctuation w_{rms}/U normal to the surface of the wing, as well as Reynolds stress correlation $\langle v'w'\rangle/U^2$, both of which are essentially coincident with maxima of the averaged vorticity $\langle\omega\rangle$ of the separated layer. Peak values of these fluctuation quantities occur well inboard of the leading edge of the wing, and their peak magnitudes continue to increase with increasing angle of attack up to a moderately high value of α. Then, at sufficiently high angle of attack, where substantial stall occurs, the peak value is actually decreased.

3) The instantaneous structure of the flow is represented by patterns of instantaneous vorticity, which take the form of well-defined concentrations. At sufficiently low angle of attack, these individual concentrations of vorticity retain their identity, whereas at moderate and moderately high values of angle of attack, both smaller-scale and larger-scale concentrations are evident. These patterns of instantaneous vorticity concentrations allow physical interpretation of the spectral content of the unsteadiness. Most of the spectral peaks along the separated vorticity layer are relatively broadband and attain maximum amplitude well inboard of the leading edge. When the averaged vorticity layer deflects toward the surface of the wing near its plane of symmetry, the spectral peaks become small or undetectable. At relatively low angle of attack, the same spectral peak persists along the vorticity layer, whereas at moderate and moderately high angle of attack, the predominant spectral peak is successively lowered with increasing distance inboard of the leading edge, where larger-scale clusters of vorticity are evident.

4) When the wing is subjected to small-amplitude perturbations, substantial alterations of both the instantaneous and time-averaged structure were observed. The most effective frequency of excitation corresponds to the subharmonic of the broadband fluctuations in the region of the shear layer closest to the leading edge, though this criterion is not necessarily universal for other geometric and flow parameters.

Acknowledgments

The authors are pleased to acknowledge support of the U.S. Air Force Office of Scientific Research (AFOSR) under Grant F49620-02-1-0061, monitored by John Schmisseur. The first author was supported jointly by AFOSR and Cukurova University during his research stay as a visiting scientist at Lehigh University. Prior to and subsequent to his stay at Lehigh, he has been supported as a research assistant at Cukurova University.

References

[1]Magness, C., Robinson, O., and Rockwell, D., "Instantaneous Topology of the Unsteady Leading-Edge Vortex at High Angle of Attack," *AIAA Journal*, Vol. 31, No. 8, 1993, pp. 1384–1391.

[2]Visbal, M. R., and Gordnier, R. E., "Cross-Flow Topology of Vortical Flows," *AIAA Journal*, Vol. 32, No. 5, 1994, pp. 1085–1087.

[3]Riley, A. J., and Lowson, M. V., "Development of a Three-Dimensional Free Shear Layer," *Journal of Fluid Mechanics*, Vol. 369, 1998, pp. 49–89.

[4]Ol, M. V., and Gharib, M., "The Passage Toward Stall of Nonslender Delta Wings at Low Reynolds Number," AIAA Paper 2001-2843, 2001.

[5]Gursul, I., Taylor, G., and Wooding, C. L., "Vortex Flows over Fixed-Wing Micro Air Vehicles," AIAA Paper 02-0698, Jan. 2002.

[6]Payne, F. M., Ng, T. T., Nelson, R. C., and Schiff, L. B., "Visualization and Wake Surveys of Vortical Flow over a Delta Wing," *AIAA Journal*, Vol. 26, 1988, pp. 137–143.

[7]Lowson, M. V., "The Three Dimensional Vortex Sheet Structure on Delta Wings," AGARD, CP 438, Paper 11, 1988.

[8]Reynolds, G. A., and Abtahi, A. A., "Three-Dimensional Vortex Development, Breakdown and Control," AIAA Paper 89-0998, 1989.

[9]Washburn, A. E., and Visser, K. D., "Evolution of Vortical Structures in the Shear Layer of Delta Wings," AIAA Paper 94-2317, 1994.

[10]Mitchell, A., Molton, P., Barberis, D., and Delery, J., "Characterization of Vortex Breakdown by Flow Field and Surface Measurements," AIAA Paper 2000-0788, 2000.

[11]Visbal, M. R., and Gordnier, R. E., "On the Structure of the Shear Layer Emanating from a Swept Leading Edge at Angle of Attack," AIAA Paper 2003-4016, June 2003.

[12]Gordnier, R. E., and Visbal, M. R., "Higher-Order Compact Difference Scheme Applied to the Simulation of a Low Sweep Delta Wing Flow," AIAA Paper 2003-0620, Jan. 2003.
[13]Gad-el-Hak, M., and Blackwelder, R. F., "The Discrete Vortices form a Delta Wing," *AIAA Journal*, Vol. 23, 1985, pp. 961, 962.
[14]Ozgoren, M., Sahin, B., and Rockwell, D., "Vortex Structure on a Delta Wing at High Angle-of-Attack," *AIAA Journal*, Vol. 40, No. 2, pp. 285–292.
[15]Winant, C. D., and Browand, F. K., "Vortex Pairing: The Mechanism of Turbulent Mixing–Layer Growth at Moderate Reynolds Number," *Journal of Fluid Mechanics*, Vol. 63, 1974, pp. 237–255.
[16]Gordnier, R., and Visbal, M. R., "Numerical Simulation of the Unsteady Vortex Structure over a Delta Wing," AIAA Paper 91-1811, 1991.
[17]Gordnier, R., and Visbal, M. R., "Unsteady Vortex Structure over a Delta Wing," *Journal of Aircraft*, Vol. 31, 1994, pp. 243–248.
[18]Gordnier, R. E., and Visbal, M. R., "Instabilities in the Shear Layer of Delta Wings," AIAA Paper 95-2281, 1995.
[19]Cipolla, K., and Rockwell, D., "Small-Scale Vortical Structures in Crossflow Plane of a Rolling Delta Wing," *AIAA Journal*, Vol. 36, No. 12, 1998, pp. 2276–2278.
[20]Garg, A. K., and Leibovich, S., "Spectral Characteristics of Vortex Breakdown Flowfields," *Physics of Fluids*, Vol. 22, 1979, pp. 2053–2064.
[21]Gursul, I., "Unsteady Flow Phenomena over Delta Wings at High Angle of Attack," *AIAA Journal*, Vol. 32, No. 2, 1994, pp. 225–231.
[22]Menke, M., Yang, H., and Gursul, I., "Experiments on the Unsteady Nature of Vortex Breakdown over Delta Wings," *Experiments in Fluids*, Vol. 27, 1999, pp. 262–272.
[23]Gad-el-Hak, M., and Blackwelder, R. F., "Control of the Discrete Vortices from a Delta Wing," *AIAA Journal*, Vol. 25, 1986, pp. 1042–1049.
[24]Ozgoren, M., Sahin, B., and Rockwell, D., "Perturbations of a Delta Wing: Control of Vortex Breakdown and Buffeting," *Journal of Aircraft*, Vol. 38, No. 6, 2001, pp. 1040–1050.
[25]Akilli, H., and Rockwell, D., "Vortex Formation from a Cylinder in Shallow Water," *Physics of Fluids*, Vol. 14, No. 9, 2002, pp. 2957–2967.

R. Lucht
Associate Editor